CORRUGATED QWIP FOR TACTICAL ARMY APPLICATIONS

David. P. Forrai, Darrel W. Endres
L-3 Communications Cincinnati Electronics
Mason, OH 45040

Kwong-Kit Choi
U.S. Army Research Laboratory
Adelphi, MD 20783

John J. O'Neill
U.S. Army RDECOM CERDEC NVESD
Fort Belvoir, VA 22060

ABSTRACT

L-3 Communications Cincinnati Electronics (CE), the Army Research Laboratory (ARL), and the Army Night Vision and Electronic Sensors Directorate (NVESD) have been developing the corrugated quantum well infrared photodetector (C-QWIP) technology for applications in tactical LWIR imaging. The C-QWIP was invented at ARL and shows promise to overcome some of the limitations in commercially available QWIPs. The C-QWIP uses micro mirrors on the detector to turn the polarization of the incident photons. This offers two distinct advantages over the grating couplers used in commercial QWIPs. The first is that the effectiveness for turning the polarization is much higher, thus higher absorption quantum efficiency is possible. Second, the reflection off the micro-mirrors is wavelength independent. This allows the material to completely define spectral response of the QWIP. CE and ARL have fabricated C-QWIP FPAs with bandwidths exceeding 3 µm, roughly 5 times wider than current commercial QWIPs. The increased bandwidth and quantum efficiency of the C-QWIP shows much promise to achieve the speed, sensitivity, and resolution needed for Army tactical systems.

1. BACKGROUND

Quantum well infrared photodetector (QWIP) technology differs from other infrared detector technology in that it relies on inter-subband absorption to create photo-carriers. The inter-subband transition is created in a quantum well (QW), which consists of a thin layer of semiconductor material sandwiched between two thicker layers of larger bandgap material. Within the quantum well, the energy levels are quantized. When the QW is doped, extra carriers (electrons are shown in Figure 1) occupy these energy states. When the material is cooled, most electrons are bound to the lowest energy state referred to as the ground state. An incident photon upon the QW elevates a carrier to a higher energy level, where the carrier is able to move freely above the barriers. This is contrasted with a direct band gap material, where an incident photon generates an electron-hole pair that can move freely within the conduction-valence bands respectively. For both types of absorption, if an electrical bias is applied, photo-current will flow.

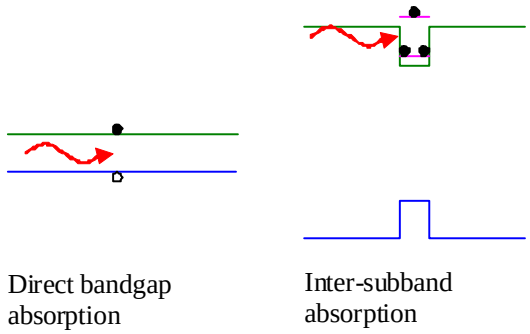

Figure 1: Illustration of the difference between direct bandgap and inter-subband absorption.

QWIP for infrared imaging has been evolving over the past twenty years. The challenge for QWIP technology has been the optical coupling requirements for detection. QWIP material is not absorptive when the light directly falls on the material surface. The optical electric field in this case is parallel to the material layers. To induce absorption, the field needs to be vertical. Several domestic and foreign sources have developed techniques for the manufacture of QWIP focal plane arrays (FPAs) and cameras. The approach they use to change the field direction is to build a two-dimensional diffraction grating on top of the detector. The geometry of this detector is illustrated in Figure 2. Over a narrow spectral band, the diffraction of incoming light will create the required vertical field. While an elegant approach, high diffraction efficiency is difficult to achieve over a limited pixel area.

Report Documentation Page

Form Approved
OMB No. 0704-0188

1. REPORT DATE	2. REPORT TYPE	3. DATES COVERED
DEC 2008	**N/A**	**-**

4. TITLE AND SUBTITLE	5a. CONTRACT NUMBER
Corrugated Qwip For Tactical Army Applications	5b. GRANT NUMBER
	5c. PROGRAM ELEMENT NUMBER
6. AUTHOR(S)	5d. PROJECT NUMBER
	5e. TASK NUMBER
	5f. WORK UNIT NUMBER
7. PERFORMING ORGANIZATION NAME(S) AND ADDRESS(ES) **L-3 Communications Cincinnati Electronics Mason, OH 45040**	8. PERFORMING ORGANIZATION REPORT NUMBER
9. SPONSORING/MONITORING AGENCY NAME(S) AND ADDRESS(ES)	10. SPONSOR/MONITOR'S ACRONYM(S)
	11. SPONSOR/MONITOR'S REPORT NUMBER(S)

12. DISTRIBUTION/AVAILABILITY STATEMENT
Approved for public release, distribution unlimited

13. SUPPLEMENTARY NOTES
See also ADM002187. Proceedings of the Army Science Conference (26th) Held in Orlando, Florida on 1-4 December 2008, The original document contains color images.

14. ABSTRACT

15. SUBJECT TERMS

16. SECURITY CLASSIFICATION OF:			17. LIMITATION OF ABSTRACT	18. NUMBER OF PAGES	19a. NAME OF RESPONSIBLE PERSON
a. REPORT	b. ABSTRACT	c. THIS PAGE			
unclassified	**unclassified**	**unclassified**	**UU**	**8**	

Furthermore, one study (De Rossi et al., 2003) showed that when the pixel size is less than 25 microns across, the entire pixel volume acts as a resonant cavity in defining the overall electromagnetic (EM) field. A small change in the pixel structure, such as its lateral and vertical dimensions, the thickness of the substrate, and the shape of the mesas, will change the detector quantum efficiency (QE) drastically. Therefore, the design of the grating cavity is much more complex in high definition FPAs. Although large QEs have been reported using this approach, there is little evidence that high performance can be reliably achieved given the normal manufacturing tolerances and varying requirements on detector spectral response. From our limited testing of commercial products and third party test data, the QE is typically less than 5% in these FPAs.

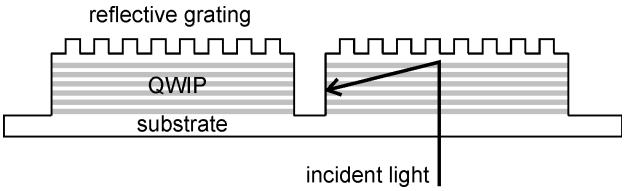

Figure 2: Illustration of the grating-coupled QWIP.

In addition to low quantum efficiency and narrow bandwidth, QWIPs operate as photoconductors. The photoconductive gain is usually less than one when using the GaAs/AlGaAs material system. The combination of low QE and low photoconductive gain yields long integration times for high-sensitivity detection even at the high flux levels of terrestrial long-wave infrared (LWIR). Thus, QWIPs don't compete well with photovoltaic LWIR detectors in terms of speed. Consequently, current commercial QWIPs have not been adopted into tactical systems for the Army.

QWIP FPAs offer some very attractive opportunities for tactical integration. The most attractive feature is dramatic cost savings on FPA manufacture by leveraging existing commercial sources for both III-V semiconductor epitaxial wafer growth and III-V semiconductor device processing. Epitaxial growth reactors are most economical when run continuously. To be cost effective, a reactor should grow a minimum of about 80 wafers per month. Because QWIPs share epitaxial growth with other military and commercial applications, the reactor can run wafer lots at a rate for very economical operation, therefore the cost per wafer is much lower than many other infrared detector technologies. In addition to low wafer cost, III-V semiconductor epitaxy is mature and offers very uniform material over large areas (100 mm and 150 mm diameter wafers are common). This leads to a very high yield of good die per wafer, along with a large number of die per wafer. It also presents the immediate opportunity to fabricate multiple very large format detector arrays on a single wafer, thus increasing the yield over other technologies that are limited by smaller wafers. Finally, equipment and processes exist to fabricate devices in III-V semiconductors. This reduces the need for custom tool and process development. Thus there is motivation to evolve QWIP technology for potential applications within the Army.

Our work in developing C-QWIP focal plane arrays (FPAs) has shown promise that this technology might be able to satisfy certain Army LWIR imaging needs. We will start by describing the C-QWIP detector, follow with test results, present some analysis that shows the performance potential of C-QWIP sensors, and draw conclusions for future work.

2. C-QWIP DESCRIPTION

The geometry of the C-QWIP is illustrated in Figure 3. The light incident on the detector propagates through the substrate and quantum well (QW) region unabsorbed until it intercepts the inclined micro-mirror. The direction of propagation is turned parallel to the QW layers where the electric field can become perpendicular to the QW layers. Assuming the incident light is unpolarized, the theoretical limit for maximum quantum efficiency (QE) is 50%.

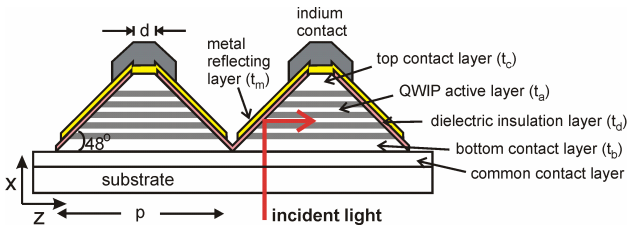

Figure 3: Illustration of the C-QWIP geometry.

C-QWIP FPAs improve the technology in both performance and manufacturability. Because reflection is more effective in redirecting the light, the QE is larger. Reflection is also independent of wavelength. This means that the detector will preserve the natural absorption spectrum of the material. Figure 4 compares the material spectrum measured at ARL to the FPA spectrum measured at NVESD. Since the material absorption bandwidth can be much wider than the grating coupling bandwidth, the integrated photoresponse of the C-QWIP can be much larger than that of grating-coupled QWIPs.

Without the need for matching the material wavelength to the grating cavity modes in the detector, the same pixel geometry and production process are applicable to all QWIP material designs. This allows the simultaneous production of FPAs having a wide range of wavelength bands without jeopardizing QE. In the absence of the fine grating features, it also allows the use of standard photolithographic techniques. With the C-QWIP structure, the production of FPAs can be faster and less expensive than all competitive long wavelength infrared technologies. The FPAs are more uniform and can be produced in very large formats. Figure 5 shows a

photograph of a fully processed C-QWIP wafer and Figure 6 shows a SEM image of the detectors.

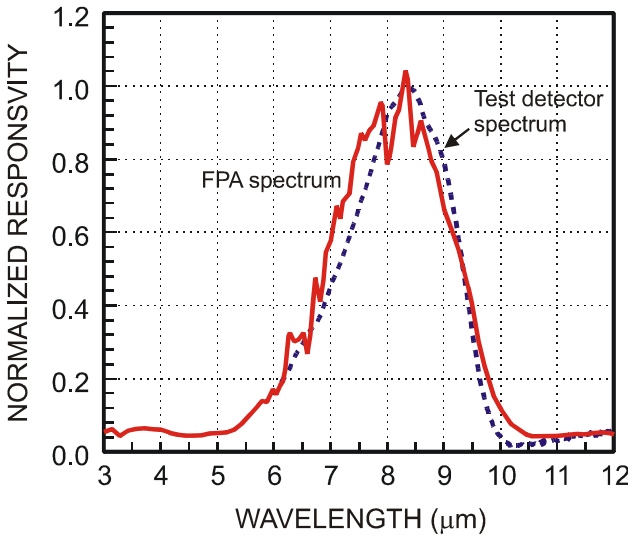

Figure 4: Comparison of material and FPA spectral response measurements.

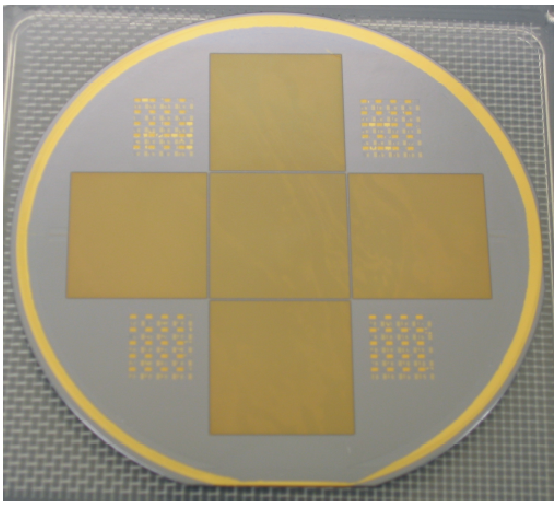

Figure 5: C-QWIP wafer with very large format arrays.

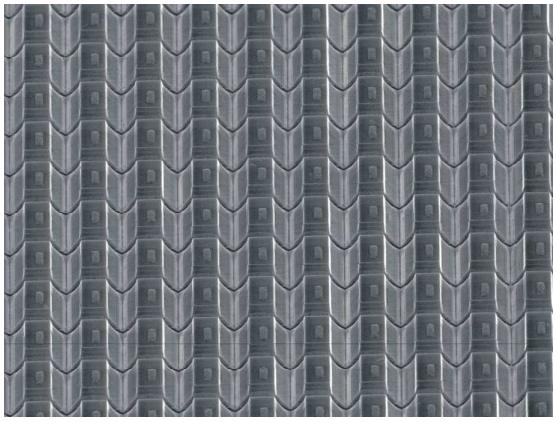

Figure 6: SEM image of the C-QWIP detectors.

3. TEST RESULTS

Our first FPA used a short cut-off material design with a FWHM bandwidth of ~1.5 μm. The calculated and measured spectrum is shown in Figure 7. This detector used 106 QW periods to maximize the absorption region in the detector. Since peak QE is inversely proportional to spectral bandwidth, we chose this narrow band design to demonstrate a high QE. The bound-to-quasi-bound (B-Q) transition in this detector yielded a very low photoconductive gain that peaks at very high bias for the 106 QWs. Figure 8 shows the measured photoconductive gain of the material. Unfortunately, the bias requirement for peak responsivity was too high for the available read-out integrated circuits (ROICs). Therefore, we characterized these detector arrays at high bias on fan-outs. At 11V detector bias, we measured a collection efficiency of 2.84%, which yields a peak QE of 36.9%. While impractical for implementation in an imager (both from the spectral response and detector bias standpoint), this work showed that high QE is possible in the C-QWIP structure. Figure 9 shows an image at a lower voltage.

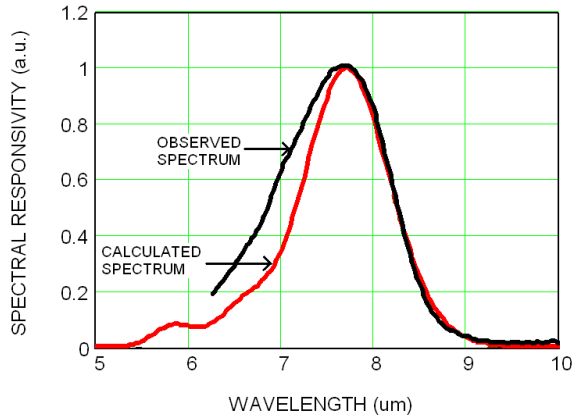

Figure 7: Calculated and measured spectrum of the first FPA.

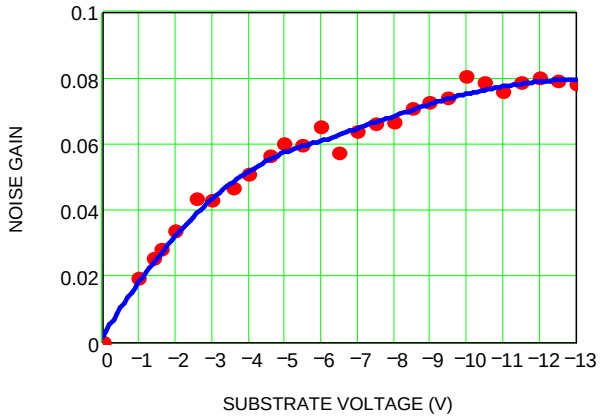

Figure 8: Photoconductive gain measurement of the first FPA material.

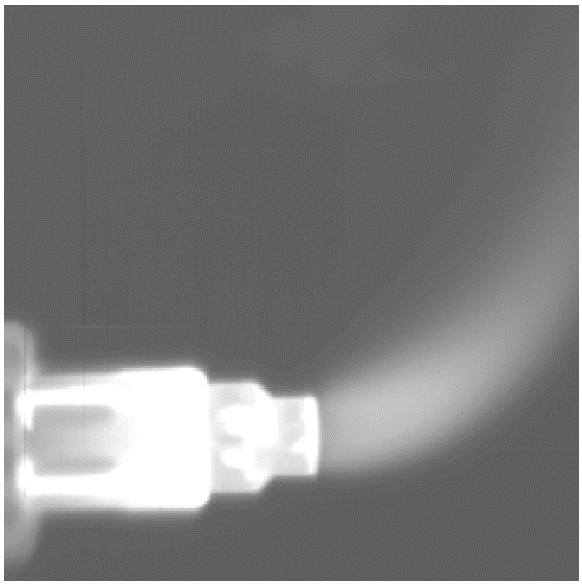

Figure 9: Image from the first FPA at 3V bias.

Our next FPA chose a different path. This design also used 106 QWs, but our goal was to obtain a broad 8 to 12 µm spectral response and to use a bound-to-continuum (B-C) transition to lower the bias requirements. The long cut-off required lower barriers in the QW design, therefore the photoconductive gain was higher than the first FPA. Figure 10 shows the spectrum and Figure 11 shows the photoconductive gain for this FPA. The full width half maximum (FWHM) bandwidth exceeds 3 µm for this FPA.

The measured CE of this FPA at 5 V detector bias was 3.9%, which leads to an extracted peak quantum efficiency of 25.8%. An image from this FPA is shown in Figure 12. While this FPA yielded excellent performance results, the long cut-off required an FPA operating temperature below 60K. Therefore, we focused our next efforts on material designs with cut-off wavelengths at or below 10 µm and a FHWM bandwidth of ~2 µm.

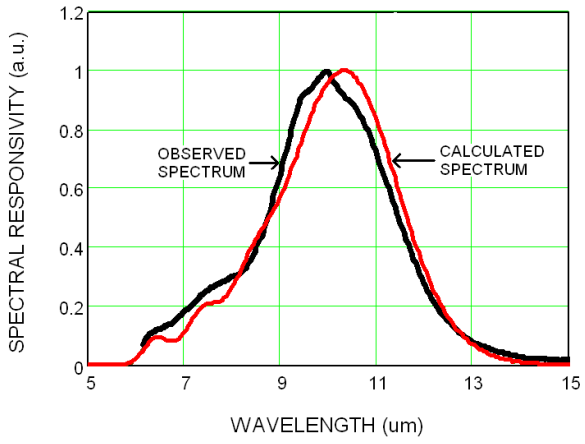

Figure 10: Calculated and measured spectral response

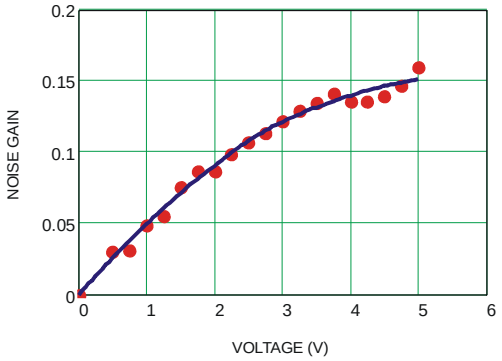

Figure 11: Photoconductive gain measurement of the second FPA material.

Figure 12: Image from the second FPA at 3V bias.

Of these materials we will highlight an FPA fabricated with a smaller pitch. Due to smaller detector geometry, the total number of QWs decreases from 106 to 92. Also, the nominal QW doping was decreased to one half that of the preceding FPAs. With lower doping and smaller pitch, we expect the QE to be lower than the previously described FPAs.

The calculated and measured spectral response of this material is shown in Figure 13. We described the transition of this material as bound-to-quasi-bound+ (B-Q+) as it lies somewhere between the previous B-Q and B-C designs. The FWHM bandwidth for this FPA is around 2 µm. It should be noted that this bandwidth is nearly 3 times as wide as the response for a grating coupled QWIP. Thus, despite an expected QE lower than the previously reported FPAs, the integrated photocurrent in this FPA will exceed that of grating QWIPs by a wide margin.

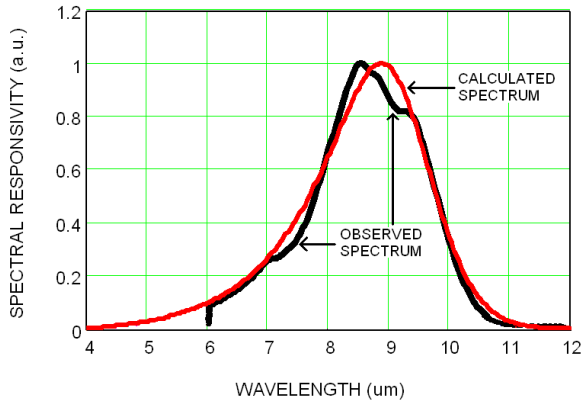

Figure 13: Spectral response of the third FPA reported in this paper.

The measured photoconductive gain is shown in Figure 14. The peak value is similar to that of the second FPA. This is reasonable since there was only a small change in the number of QWs and the doping density is not expected to make a significant impact in photoconductive gain.

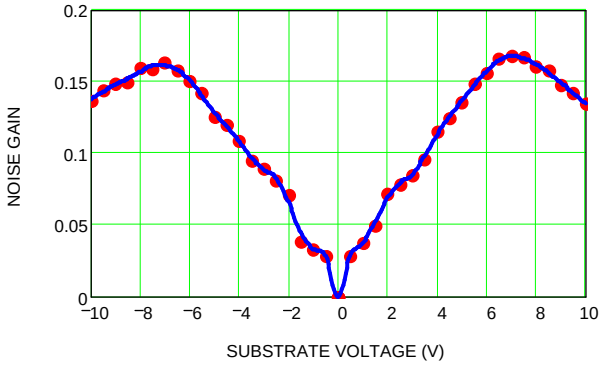

Figure 14: Photoconductive gain measurement of the third FPA material.

Figure 15 shows an image taken using the third FPA described. Measurements on this FPA were performed at both CE and NVESD. CE obtained an average conversion efficiency of 2.3%, which translates to a peak QE of 14.7%. This is in excellent agreement with theoretical predictions. At NVESD, an average conversion efficiency of 2.23% was obtained, in excellent confirmation with CE's measurements.

A median NETD of 35 mK was measured for this FPA at NVESD. While not an overly impressive sensitivity, this value is not indicative of the true FPA capability. The video collection system for this FPA was primitive compared to a tactical sensor and therefore added significant noise to the video. For this reason, nether CE nor NVESD were able to extract photoconductive gain from FPA measurements and confirm ARL's results from material characterization.

Figure 15: Image from the third FPA at 7V bias.

In all three FPAs, excellent sensitivity and resolution were demonstrated. For a more detailed description of the material design, theoretical predictions, and FPA parameters, please review the second reference (Choi et al., 2008).

4. C-QWIP SENSOR ANALYSIS

We have developed models for the QWIP sensor based on theoretical performance of QWIPs (Choi et al., 2007) and verified through our FPA characterization. From this model, we have established a sample performance specification for a tactical sensor and exercised our model to determine the required peak QE, conversion efficiency and well size to achieve that specification. Finally, we compare the results of a commercial QWIP and our C-QWIP FPAs to see how closely they meet the desired performance. The following sections will describe this analysis.

1. Performance Specification

We establish two levels of performance for our sensor. The first is considered the minimal sensitivity and speed needed for typical ground applications and the second is the desired performance. The first sets the integration time of 5 msec with an NETD of 25 mK against a 300 K background. The second sets the integration time to 2 msec with an NETD of 20 mK for the same background.

The system is assumed to use an f/2.0 optic, have a total optical transmission (lens, dewar window, and cold filter) of 0.7, total fixed electronic noise equivalent to 900 electrons, and is spectrally limited from 8 µm to 13 µm. The pixel pitch is 20 µm with a fill factor of 81%. The detector is assumed to be cooled sufficiently such that the dark current to photocurrent ratio against the 300 K background is 0.1.

2. Grating-coupled QWIP Analysis

The first QWIP we consider is a grating coupled QWIP. Figure 16 shows the spectrum for this QWIP, which is representative of most commercially available QWIP FPAs. The peak response is at 8.6 µm and the FWHM spectral bandwidth is 0.7 µm.

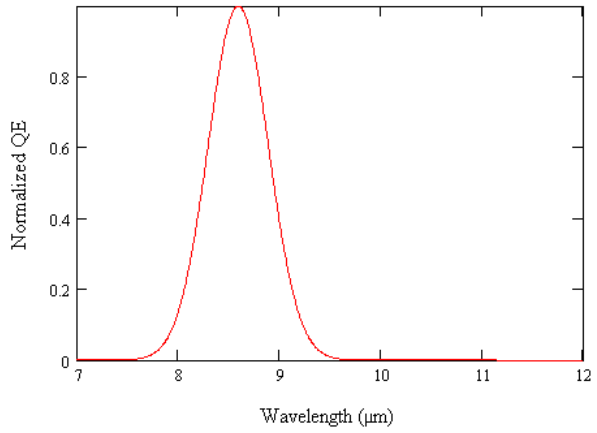

Figure 16: Spectrum representative of a typical grating-coupled QWIP.

Figure 17 shows the results using this spectrum and our performance specification plotted as a function of material photoconductive gain. The peak QE needed to attain the minimal performance is plotted using a solid line while the peak QE needed to attain the desired performance is plotted using the dashed line. Note that at small (< 0.2) photoconductive gains, the required peak QE to obtain the desired performance increases rapidly. Since QE is theoretically limited to 100%, the analysis shows that there are values for photoconductive gain where the narrow band detector can't achieve either performance spec. As photoconductive gain increases, the required peak QE decreases but at a slow rate.

The dot plots published data for a typical commercial QWIP with a 30 µm pitch. Note that this pitch is larger than the hypothetical sensor and, as stated previously, the QE can degrade considerably when the pitch is less than 25 µm. We conclude from this data that if a material system with much higher gain is used in the grating-coupled QWIP, it may be possible to satisfy the minimum performance, however, to reach the desired performance, the peak QE would have to exceed 60%, which to our knowledge has never been demonstrated in a grating-coupled QWIP.

Another important consideration is the well size requirement of the ROIC versus the photoconductive gain of the detector. This data is plotted in Figure 18. For this plot, we assume that the well is filled at a 60° C background temperature. Note that for the published photoconductive gain of 0.2, the well size requirement for the 20 µm detector is reasonable. However, as the photoconductive gain increases, the required well size grows beyond that of typical ROICs. Thus, if a grating-coupled QWIP with high photoconductive gain was built to meet the minimal performance specification, an appropriate ROIC would also need to be built to provide the required well fill.

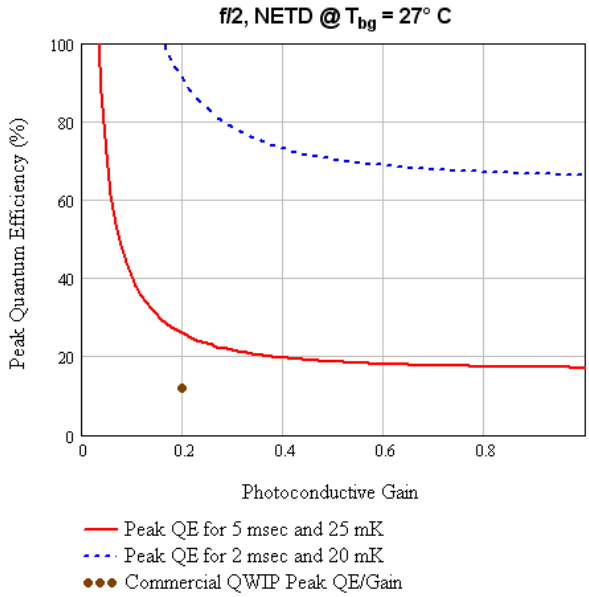

Figure 17: Model results for the grating-coupled QWIP.

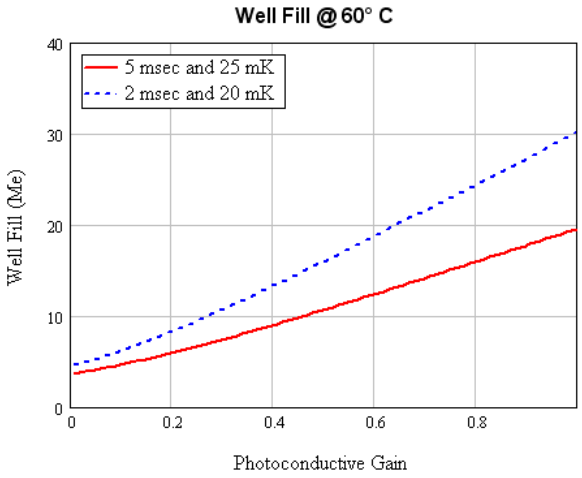

Figure 18: Model results for well fill against a 60° C background.

3. 10 µm Cut-off C-QWIP Analysis

Our next analysis used a spectrum representative of several different material iterations for the C-QWIP with a cut-off around 10 µm. The spectrum used in this analysis is shown in Figure 19. The results of our sensor model are shown in Figure 20. The first thing to note is how the increased bandwidth of the C-QWIP detector dramatically decreases the peak QE requirement to

achieve the desired performance. We hypothesize that the required peak QE is inversely proportional to bandwidth.

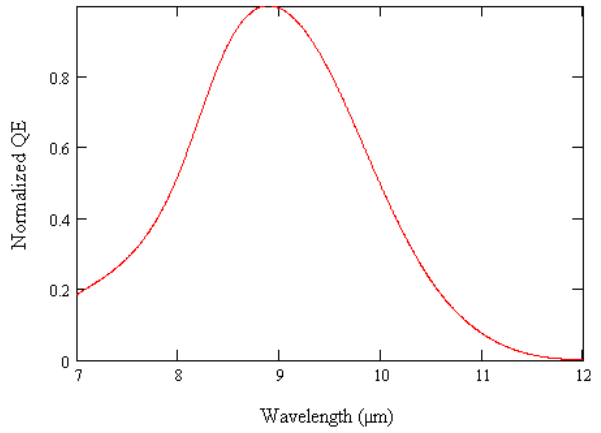

Figure 19: Spectrum representative of numerous 10 µm cut-off C-QWIP FPAs fabricated.

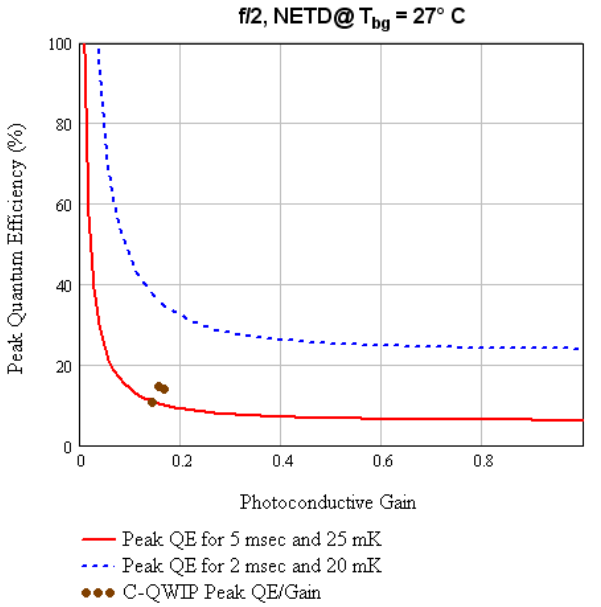

Figure 20: Model results for the C-QWIP sensor with a 10 µm cut-off detector.

The dots in Figure 20 represent the measured QE from three different C-QWIP FPAs. These FPAs varied in number of QWs, doping density in the QWs, and detector pitch (either 20 µm or 25 µm). It should be noted that none of them had the full doping and maximum number of QWs of the first and second FPAs described. It shows that the minimum requirement is met by these FPAs. All FPAs had photoconductive gains around 0.15. To meet the desired performance, the peak QE will need to be around 35%. We feel that with time and further development, an appropriate peak QE and photoconductive gain can be reached such that a detector with a cut-off around 10 µm will be able to achieve the desired performance.

The well size requirement versus photoconductive gain for this detector is very similar to that of the grating-coupled QWIP analysis. Since the well size requirements are only slightly higher, we chose not to add that plot to this paper.

4. 12 µm Cut-off C-QWIP

The spectrum of our broadband C-QWIP is shown in Figure 21 and corresponding model results are shown in Figure 22. As we hypothesized, the wider bandwidth lowers the required peak QE from that of the previously analyzed QWIPs.

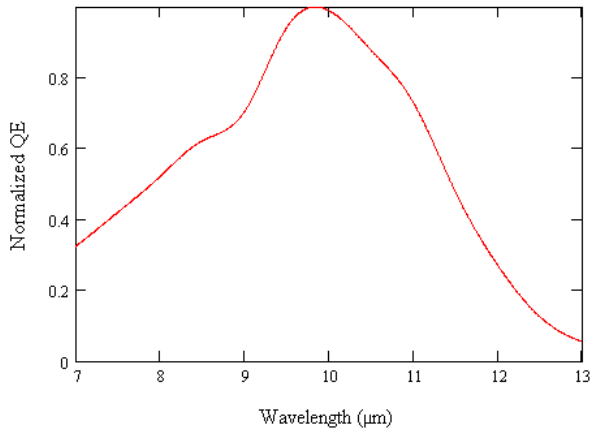

Figure 21: Spectrum of the broadband 12 µm cut-off C-QWIP FPA.

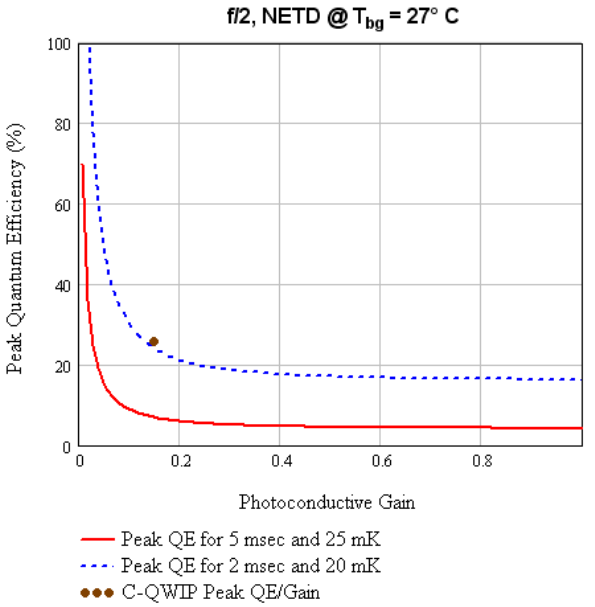

Figure 22: Model results using the spectral response of our broadband C-QWIP FPA.

The dot on Figure 22 represents the measured performance of the broadband C-QWIP. It was the only FPA that could attain the desired performance. We should

note that its pitch is 25 µm, so a similar device on a 20 µm pitch per our hypothetical system may perform differently. However, our detector model indicates that the peak QE of a 20 µm pixel and a 25 µm pixel differs only by 8% for the same number of QWs. Therefore, we expect the broadband material on the 20 µm pitch could meet the desired performance goal as well.

Figure 23 shows the required well fill versus photoconductive gain assuming saturation at a 60° C background. For gains < 0.2, the well size is reasonable for the 20 µm detector using current ROICs. Despite the significantly wider bandwidth than the grating-coupled QWIP, the relative increase in required well size between the two is small.

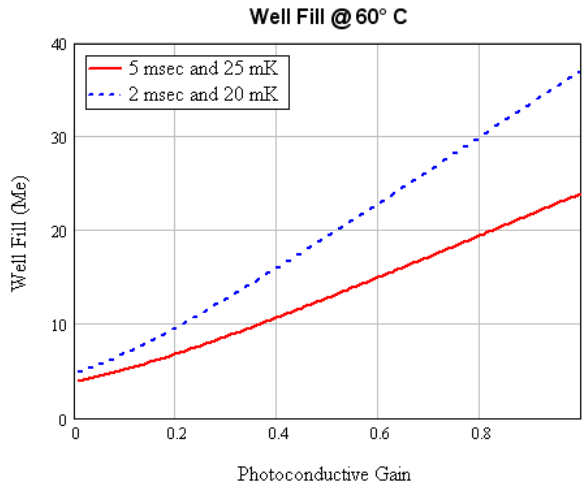

Figure 23: Well fill requirements for the broadband C-QWIP in the sensor.

5. FUTURE WORK

From the FPAs we fabricated and characterized, and from our sensor model, we conclude that a maximum number of QWs (~100), full doping, a FWHM bandwidth greater than 2 µm, and a B-C transition in the GaAs/AlGaAs material are required to meet the desired performance goal. For a B-Q transition, the bias requirements are too high and the photoconductive gain of the material too low to achieve the desired performance. The B-Q+ transition may also yield acceptable performance, however, further development work is required to ascertain its viability.

For the near term, our goal is to produce an FPA that will achieve the desired performance in an existing sensor, which may not exactly match that of the hypothetical sensor described. To do this, we will use a broadband material similar to that of the second FPA described. However, for the long cut-off wavelength, the operating temperature of the FPA may be lower than desired for a tactical sensor. We have two approaches for achieving higher operating temperature.

The first will continue using the GaAs/AlGaAs material system, and focus on the material design to find the shortest cut-off wavelength to achieve the goal. From our work, we believe this will fall around 10.5 µm. Our second approach will look at alternate material systems for higher photoconductive gain. A previous study (Razeghi et al., 2001) showed that the InGaAs/InP material system can yield a photoconductive gain ~10× higher than the GaAs/AlGaAs system. Fortunately, InP epitaxy, although not as mature as GaAs epitaxy, is being used in commercial applications so much of the resources available for GaAs epitaxy and wafer processing also support InP. Using the InGaAs/InP material system would push our current ~0.15 photoconductive gain to ~1.0, and lower our required peak QE to the low 20s %. This should be quite achievable in a C-QWIP with a cut-off wavelength below 10 µm. However, along with this material system change, a new ROIC with much higher well fill will need to be designed and fabricated.

CONCLUSION

We have fabricated, characterized, and analyzed several C-QWIP FPAs for potential use in Army tactical systems. While further development is still needed, our work to date shows much promise that the C-QWIP can achieve the performance needed for these sensors. The C-QWIP appears to be well positioned to provide the Army with very large format, LWIR imagers currently unattainable using alternate IR technologies.

ACKNOWLEDGEMENTS

This work has been supported by MDA, NASA, and NVESD.

REFERENCES

Choi, K.K.; Devitt, J.W.; Forrai, D.P.; Endres, D.; Marquis, J.; Bettge, J.; and Pinsukanjana, P.; 2007: C-QWIP material design and growth, *Proc. SPIE*, **6542**, S1 – S11

Choi, K.K.; Forrai, D.P.; Endres, D.; Sun, J.; Pinsukanjana, P.; and Devitt, J.W.; 2008: C-QWIP focal plane array development, *Proc. SPIE*, **7082**, submitted for publication

De Rossi, A.; Costard, E.; Guerineau, N.; and Rommeluere, S.; 2003: Effect of finite pixel size on optical coupling in QWIPs, *Inf. Phys. & Tech.*, **44**, 325-330

Razeghi, M.; Erdtmann, M.; Jelen, C.; Guastavinos, F.; Brown, G. J.; Park, Y. S.; 2001, Development of quantum well infrared photodetectors at the center for quantum devices, *Inf. Phys. & Tech.*, **42**, 135-148